Anal. Bioanal. Electrochem., Vol. 15, No. 11, 2023, 1001-1017
https://www.doi.org/10.22034/abec.2023.709116

Analytical & Bioanalytical Electrochemistry

Full Paper

Improvement of Photoelectrochemical Water Splitting Performance by Electrochemical Synthesis of Cu-Doped Zno Nanotubes Decorated with Silver Nanoparticles

Tahere Mollaei, and Ahmad Rouhollahi*

Faculty of Chemistry, K.N. Toosi University of Technology, Tehran, Iran

*Corresponding Author, Tel.: (+98) 23064222
E-Mail: rouhollahi@kntu.ac.ir

Received: 8 October 2023 / Accepted with minor revision: 25 November 2023 / Published online: 30 November 2023

Abstract- Cu-doped ZnO nanotube arrays decorated with silver nanoparticles (ZnO NTs: Cu/Ag) were synthesized on fluorine-doped tin oxide (FTO) substrates by electrodeposition technique and used as photoanodes to investigate photoelectrochemical (PEC) water splitting efficiency under visible light irradiation. The prepared photoanodes were characterized by field emission scanning electron microscope, energy-dispersive X-ray spectroscopy, X-ray diffraction, and UV-Visible absorption spectroscopy. Linear sweep voltammetry, electrochemical impedance spectroscopy, and Mott-Schottky analysis were used to evaluate PEC efficiency. The ZnO NT: Cu/Ag photoanode exhibits a significant photocurrent density of about180 µA/cm2 at 1.6 V vs. RHE compared to other films. Also, the results show that the charge transfer density increases to 1.03×1022cm-3 and the charge transfer resistance decreases to 17.6 Ω. The improved PEC performance of ZnO NTs: Cu/Ag is attributed to the localized surface plasmon resonance (LSPR) effect of Ag nanoparticles, the ability of Cu to absorb visible light, efficient separation, and transfer charge carriers.

Keywords- Ag nanoparticles; Electrodeposition; Cu-doped ZnO nanotube; Photoanode; Photoelectrochemical water splitting

1. INTRODUCTION

Today, the energy crisis and problems of environmental pollution and the use of clean energy have become an important challenge for mankind. Recently, photoelectrochemical (PEC) water splitting is one of the most promising strategies to produce hydrogen and oxygen

as valuable and fresh fuel [1,2]. Metal oxide semiconductors have characteristics such as environmentally friendly, stable, cheap, wide bandgap, and easy, so they are often used as photoanodes in PEC systems [3,4]. ZnO has attracted much attention compared to other semiconductor oxides due to its high carrier mobility, low cost, non-toxicity, high thermal and chemical stability [5]. Therefore, it plays a vital role in many applications such as electronics, biosensors, optoelectronics and solar cells [4,6]. Different structures of ZnO have been used for PEC water splitting, including three-dimensional branched nanowires [7], nanorods (NR) [8], nanowires [9], ZnO nanotrees and nanocluster structures [10] and starlike structures [11]. In the past decades, studies have shown that one-dimensional (1D) nanostructures (such as nanorods, nanowires, and nanotubes) improve the charge carrier transport due to their high surface area and efficient charge transport, so they are considered as one of the best candidates for photocatalyst applications in the PEC systems [5]. However, despite the numerous advantages of ZnO, the use of ZnO in photocatalytic applications was usually limited due to its low efficiency in the range of the visible light spectrum and fast recombination of charge carriers because of its broad band gap (~ 3.2 eV) [12,13]. Many studies have been conducted to overcome these limitations, such as metal or nonmetal doping, nanostructure engineering and surface modification [14–18]. Recently, metal ion doping and metal nanoparticle (NP) decoration are good and promising options for changing the electrical and optical properties of ZnO. The photocatalytic activity of metal-modified ZnO and nanoparticle-decorated ZnO has been widely studied by researchers [19,20]. Doping with metal ions creates an impurity level below the conduction band or above the valence band, which acts as donor or acceptor level, respectively, which ultimately reduces the band gap and recombination rate of charge carriers [21–23]. It seems that Cu^{2+} ion can be selected as a doping element to reduce electron-hole pair recombination due to the slight difference between the ionic radius of Zn^{2+} and Cu^{2+} [21]. On the other hand, noble metals (such as Au, Ag, and Pt NPs) can significantly improve light absorption in the visible light regions based on the localized surface plasmon resonance (LSPR) effect [24-29]. Surface plasmons arise from the collective oscillation of surface free electrons of conducting metals when the frequency of photons corresponds to the natural frequency of surface electrons oscillating [24, 30-32]. Plasmonic metal NPs absorb visible light through LSPR and then generate hot electrons. In photocatalysts of semiconductors decorated with plasmonic metal NPs, the plasmon-induced hot electrons can be transferred from the plasmonic metal NPs to the conduction band of the semiconductor [33,34], which increases PEC water splitting performance. Meanwhile, Ag is superior to other noble metals with a significant quality factor in the range of 0.3-1.2 μm [35].

In this study, we use a simple and cost-effective electrodeposition technique to prepare Cu-doped ZnO nanotube arrays decorated with Ag nanoparticles (ZnO NTs: Cu/Ag) on FTO glass substrates. The properties of prepared samples are surveyed by field emission scanning electron microscope, energy-dispersive X-ray spectroscopy, X-ray diffraction and UV-Visible

absorption spectroscopy. The photoelectrocatalytic behavior of zinc oxide NT: Cu/Ag photoanode toward water splitting was investigated in the visible light region. Also, the effect of Cu doping and Ag decoration on ZnO NTs on PEC performance was studied.

2. EXPERIMENTAL SECTION

2.1. Chemical substances

All operated reagents and chemicals used in this work were analytically graded and were utilized directly without any further purification. Zinc nitrate hexahydrate ($Zn(NO_3)_2 \cdot 6H_2O$), acetone, 2-propanol, sodium nitrate ($NaNO_3$), hexamethylenetetramine (HMTA, $C_6H_{12}N_4$), sodium citrate ($C_6H_5Na_3O_7$), silver nitrate ($AgNO_3$), potassium nitrate (KNO_3) and sodium sulfate (Na_2SO_4) were purchased from Merck Company. Also, the fluorine-doped tin oxide (FTO, F-doped SnO_2) glass substrate (with the resistance of 8-10 Ω and an area of 10 mm × 10 mm) was bought from Nano Gostar Sepahan Company.

2.2. Preparation of photoanodes on FTO substrate

All photoanodes were synthesized by electrodeposition method in a three-electrode system including FTO glass substrate (with a geometric area of 1 cm^2) as working electrode, Pt plate as counter electrode and Ag/AgCl (3.0 M KCl) as reference electrode. The working electrode was rinsed in an ultrasonic bath by consecutively immersion in 2-propanol, acetone and deionized water (10 min each) before use. ZnO NR sample was prepared from aqueous solution containing 1.0 mM HMTA, 1.0 mM $Zn(NO_3)_2 \cdot 6H_2O$ and 0.1 M $NaNO_3$ in two-step potentiostatic electrolysis. First, a seed layer for nucleation of ZnO was grown on the FTO glass substrate by applying a high potential of -1.3 V for 0.5 s vs. Ag/AgCl, followed by the potential was fixed at -1.0 V vs. Ag/AgCl for 60 min to the vertical growth of ZnO nanostructures. The temperature of the electrolyte bath was kept constant at 80 °C during electrodeposition. To obtain ZnO NT photoanode, the synthesized ZnO NR photoanode was immersed in an alkaline solution of potassium hydroxide (KOH) with optimized concentration (0.125 M), temperature (85 °C) and time (20 min) respectively. ZnO NR arrays were etched to form ZnO NTs (shown in Figure S2).

Also, in the next step, electrodeposition method was used for the synthesis of Cu-doped ZnO NT photoanode. First, the Cu-doped ZnO NR sample was electrodeposited from an aqueous solution containing 1.0 mM $Zn(NO_3)_2.6H_2O$, 1.0 mM HMTA, 0.1 M $NaNO_3$ and $CuSO_4$ (4μM) in two-step potentiostatic electrolysis as previously mentioned. Then, the synthesized Cu-doped ZnO NRs was immersed in KOH solution with optimized concentration, temperature and time (0.125 M, 85 °C and 20 min), respectively. Finally, ZnO NTs: Cu photoanode was obtained after etching procedure.

Electrodeposition of Ag NPs on Cu-doped ZnO NTs was performed according to the literature [36] in an aqueous solution containing 0.05 mM $AgNO_3$, 0.1 M KNO_3, and 0.2 mM $C_6H_5Na_3O_7$ in two-step potentiostatic electrolysis. In this way that the nucleation potential was −0.8 V for a time of 100 s, and the growth potential was −0.1 V for a deposition time of 500 s, 700 s and 900 s (shown in Figure S3).

2.3. Characterization

The morphology of the nanostructures was characterized by Field emission scanning electron microscope (FESEM). The chemical composition of the samples was examined by the energy-dispersive X-ray spectroscopy (EDX). FESEM and EDX analysis were done using a MIRA3 (Tescan Company) instrument. X-ray diffraction (XRD) patterns were employed to analyze the crystalline phases of prepared films by a Panalytical X'Pert Pro diffractometer equipped with a Cu Kα irradiation (λ = 1.5406 Å). A UV-4802 double beam UV/Vis spectrophotometer (Shimadzu Company) was used to study the optical properties of samples at room temperature.

2.4. Photoelectrochemical experiments

The PEC activities were evaluated using a three-electrode configuration connected to a potentiostat/galvanostat (Autolab PGSTAT30). Prepared photoanodes (with the geometric area of 1 cm^2), Ag/AgCl (3.0 M KCl) and Pt plate acted as working electrode, reference electrode and counter electrode, respectively. All the measured potentials vs. Ag/AgCl were converted to the reversible hydrogen electrode (RHE) scale. Linear sweep voltammetry (LSV) and electrochemical impedance spectroscopy (EIS) measurements were carried out in 0.5 M Na_2SO_4 electrolyte under dark and light illumination. In addition, A white LED light was used as a light source (100 W and with intensity of 5 mW/cm^2) in the visible light irradiation.

3. RESULTS AND DISCUSSION

3.1. EDX, FESEM and XRD analysis

EDX analysis of all samples is shown in Figure 1 (a–d). In Figures 1a and b, ZnO NR and ZnO NT samples mainly contain Zn and O elements. While in Figure 1c, after Cu doping, in addition to Zn and O elements, the peak of Cu appears in the spectrum. Furthermore, in Figure 1d, in addition to the above elements, the peak of Ag can also be seen, which confirms the presence of Ag element. The Sn peak is observed in the EDX spectra of all films, which originates from the constituents of the FTO substrate. Also, the obtained results are consistent with the EDX mapping images (shown in Figure 1e) and these images confirm that all elements are homogeneously dispersed.

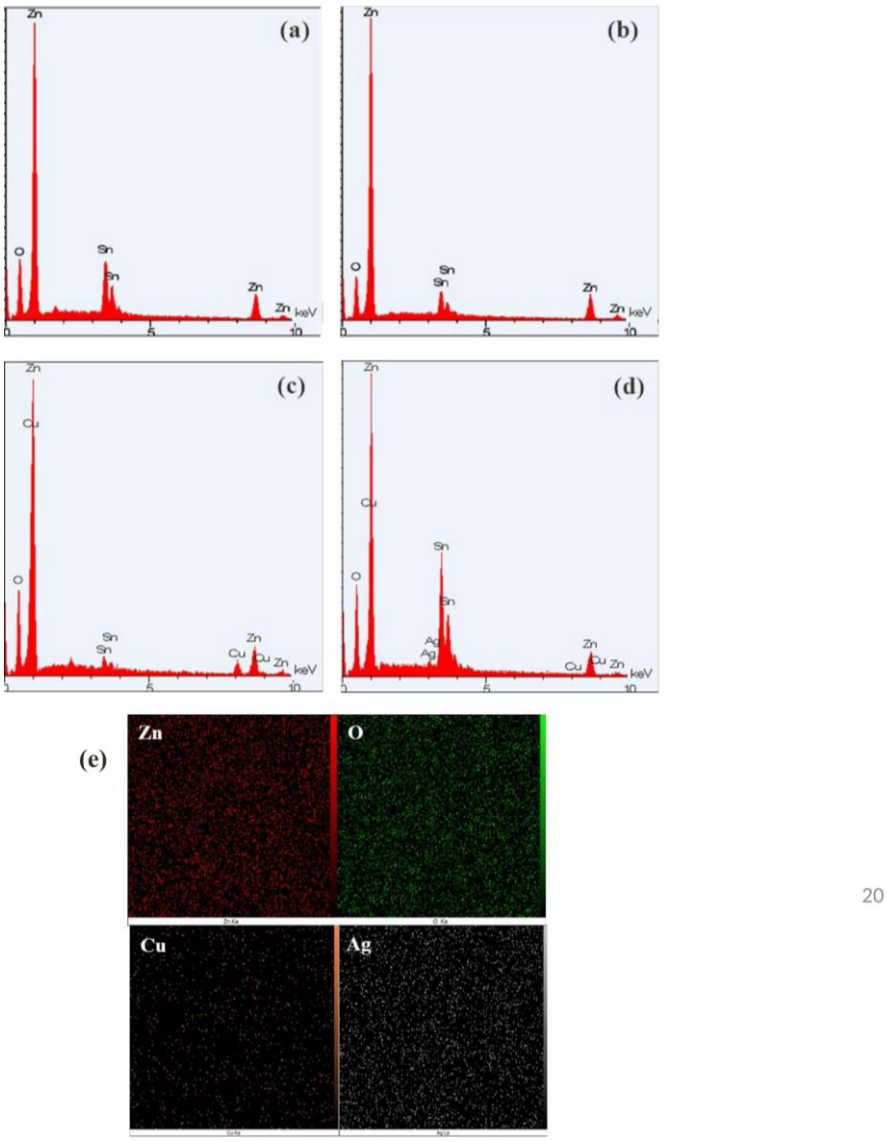

Figure 1. EDX patterns of (a) pure ZnO NRs, (b) ZnO NTs, (c) ZnO NTs: Cu, (d) ZnO NTs: Cu/Ag and (e) EDX mapping of elements in Cu-doped ZnO NTs decorated with Ag

FESEM images were used to investigate the morphological characteristics of prepared films on FTO substrate. Figure 2a and b indicate the vertically well-aligned nanorods growth throughout the substrate surface with a smooth surface and hexagonal shapes. Figure 2c and d display the ZnO NTs with well-aligned and hexagonal structures that obtained from ZnO NRs after the etching process. The formation mechanism of ZnO NTs is that first, ZnO NRs are synthesized on the FTO substrate and then they are converted into ZnO NTs during the etching process [37-41]. Figure 2e and f show Cu-doped ZnO NT films, and it is clear that their diameter is smaller than that of ZnO NR and ZnO NT samples. Since the formation of ZnO depends on the generation of OH^- ions produced at growth temperatures above 50 °C [42], the growth of Cu-doped ZnO can be faster as the concentration of OH^- ions is increased and can be an important factor in reducing the diameter of Cu-doped ZnO NTs. Also, it has been

reported that during growth of ZnO, Cu ions can enhance the growth rate and coalescence process for ZnO arrays by increasing the density of nucleation site in the seed substrate [43]. On the other hand, the diameter contraction could be due to the substitution of Zn^{2+} ions by smaller Cu^{2+} ions. In the next step, Cu-doped ZnO NTs are used as a substrate for Ag deposit and Ag NPs are grown on the surfaces of Cu-doped ZnO NTs (Figure 2g and h).

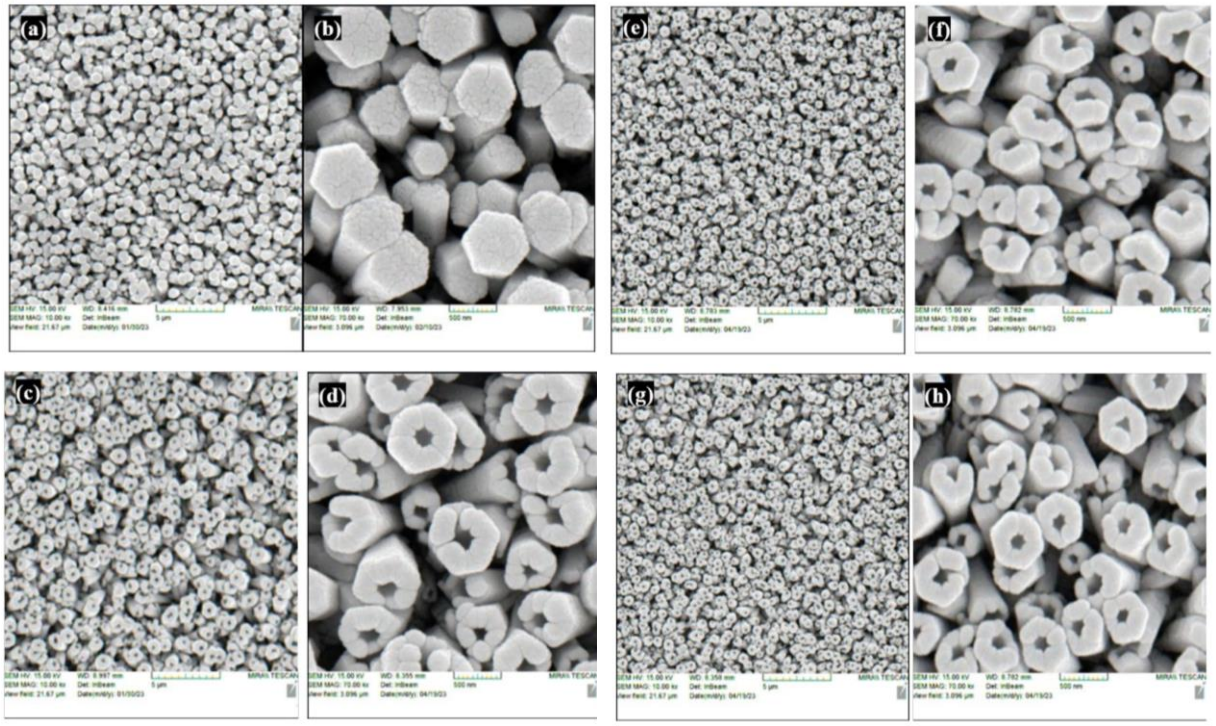

Figure 2. FESEM images of (a, b) pure ZnO NRs, (c, d) ZnO NTs, (e, f) ZnO NTs: Cu and (g, h) ZnO NTs: Cu/Ag

XRD was used to examine the phase composition and crystallographic structure of photoanodes. Figure 3 reveals that the XRD peaks of samples are narrow and sharp, indicating the good crystalline properties of the films. All the films indicate strong (002) peaks, showing preferential growth along the (001) direction. Figure 3a demonstrates the XRD pattern of ZnO NRs grown on FTO substrate. The ZnO NRs exhibiting the peaks at 2θ = 31.73°, 34.43°, 36.28°, 47.58°, 56.78°, 63.03° and 68.03° were assigned to (100), (002), (101), (102), (110), (103) and (112) planes of the wurtzite hexagonal ZnO crystal structure, which are in good agreement with the standard data of pure ZnO (JCPDS card number: 36-1451) [44]. It is also clear that nanotubes (shown in Figure 3b) display peaks at the same position as the nanorods, and no additional peaks are observed [45]. In addition, in Figure 3a and b, no other peaks pertaining to impurities were detected in the samples, indicating that no phase separation was formed, and the wurtzite hexagonal structure of the photoanodes was not changed. In Figure 3c, the intensity of the (002) peak decreases by Cu doping in a sample, indicating that Cu incorporation affects the crystallinity of ZnO and reduces its crystallinity [46]. This reduction

can be due to the replacement of Zn^{2+} ions with Cu^{2+} in ZnO crystal structure, which have almost similar ionic radius [47,48]. Figure 3d shows three small additional diffraction peaks at 37.76°, 44.31°, and 64.46° that correspond to (111), (200) and (220) crystal planes of metallic Ag (JCPDS ICDD 04-0783) [36]. It is worth mentioning that the observed peak at around 37.76 is the overlapping of SnO_2 from the FTO substrate and Ag [49].

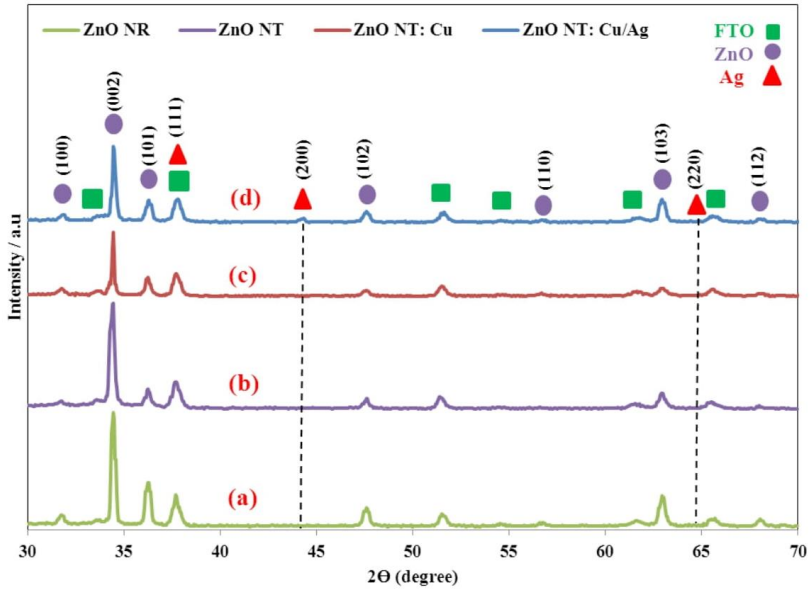

Figure 3. XRD patterns of (a) pure ZnO NRs, (b) ZnO NTs and (c) ZnO NTs: Cu and (d) ZnO NTs: Cu/Ag

3.2. UV-Visible spectra

UV–Vis absorption spectroscopy was performed to assess the optical properties and obtain the energy band gap (E_g) of the prepared photoanodes in a wavelength range of 350-700 nm at room temperature. The UV-Vis spectra of all the films are shown in Figure 4a. As seen, due to low scattering or absorption losses, all semiconductors have high transparency in the visible range and show good optical quality of the crystals. The Tauc formula was used to determine the optical absorption data of the samples (Figure 4b) [50]:

$$\alpha h\nu = A\,(h\nu - Eg)^n \qquad (1)$$

where A is constant, α is the absorption coefficient, hν is the energy of the light, E_g is the band gap and n is an index so that n = 1/2 for the allowed direct band. The values of band gaps are obtained by extrapolating of the absorption bands to the x-axis (results in Table 1). The absorption edge of the ZnO NRs is observed at about 385 nm, which corresponds to a band gap of 3.27 eV. As seen in Table 1, the band gap value of ZnO NT became narrower than that of ZnO NR photoanodes. Furthermore, the values of band gap are reduced in ZnO NTs: Cu and

ZnO NTs: Cu/Ag samples. The reduction of band gap in ZnO NTs: Cu sample is mainly caused by the closely matching energy level of localized 3d electrons of doped Cu and 2p bands of O atoms [51,52]. Cu-doped ZnO NTs after decorating with Ag NPs showed strong surface plasmon absorption in the visible light region, which is attributed to the presence of Ag NPs. It is obvious that the presence of Cu and Ag NPs together in ZnO can enhance the light absorption, which is useful for the photocatalytic performance.

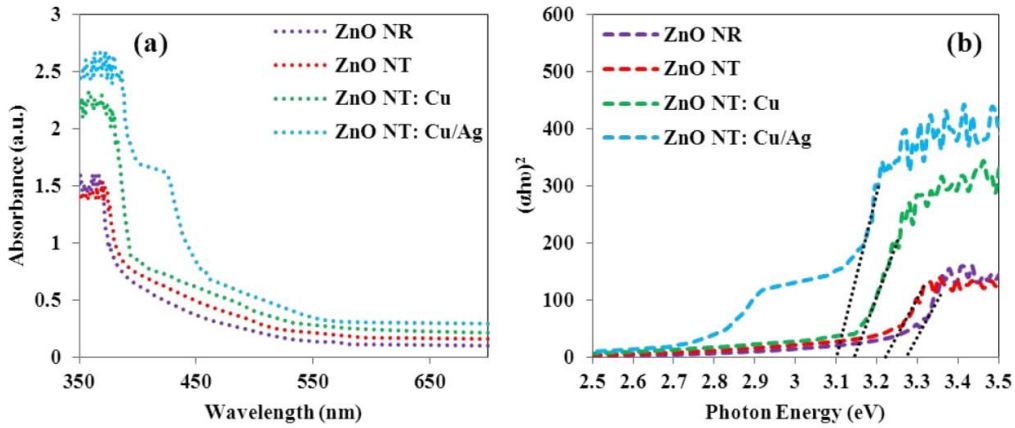

Figure 4. (a) Optical absorption spectra, (b) Band-gap of ZnO NRs, ZnO NTs, ZnO NTs: Cu and ZnO NTs: Cu/Ag

Table 1. The band gap of selected samples

Samples	Band gap (eV)
ZnO NRs	3.27
ZnO NTs	3.22
ZnO NTs: Cu	3.14
ZnO NTs: Cu/Ag	3.10

3.3. PEC measurement of photoanodes

To evaluate the PEC water splitting performance of the samples, LSV voltammograms were recorded using a three-electrode electrochemical system in 0.5 M Na_2SO_4 electrolyte solution in the dark and visible light region (shown in Figure 5a). It is clear that dark scans display negligible photocurrent density compared with light scans and the prepared photoelectrodes are inactive under dark conditions. As seen, under light irradiation, the photocurrent densities of all films are gradually enhanced in the potential range from 0.4 to 1.6 V vs. RHE. The ZnO NTs has the higher photocurrent density than the ZnO NRs under visible light illumination. The increase in the photocurrent density of ZnO NT sample can be due to

reduction of the band gap, which results in increased visible light absorption. In addition, Cu doping in ZnO NTs shows higher photocurrent density of about 27.3μA/cm^2 at 1.6 V vs. RHE than ZnO NTs, which confirms the role of Cu in improving PEC water splitting. Also, after modifying the ZnO NTs by decorating with Ag NPs, the photocurrent density reaches 48.3μA/cm^2 at the same potential. The maximum photocurrent density is observed for the photoanodes under the multi-modification of Cu doping and Ag decoration on the ZnO NTs (about180 μA/cm^2). These results show that Ag NPs decorated on the ZnO NTs: Cu can effectively improve PEC efficiency based on the plasmonic-enhanced light absorption.

Figure 5a also demonstrates the effect of electrodeposition time of Ag NPs on the improvement of PEC water splitting. The deposition time of 800 s was considered as the best response due to the increase in the density of charge carriers and efficient separation of charge carriers. The results indicate that with increasing deposition time and overloading of Ag NPs, agglomerated Ag NPs would form on the top of ZnO NTs without much deposition of Ag NPs along tube walls, which leads to decrease of the plasmon effect of Ag NPs and thus decreases PEC water splitting efficiency [53,54]. In addition, the increase of the Ag loading creates a short circuit that sucks electrons, and as a result, even with higher Ag loading, higher photocurrent density cannot be achieved [49]. Figure 5b displays the on/off cycles of the LSV with a rapid jump in photocurrent after light irradiation, and the results are in good agreement with the LSV in Figure 5a. Table 2 displays comparison of the present work with other published reports.

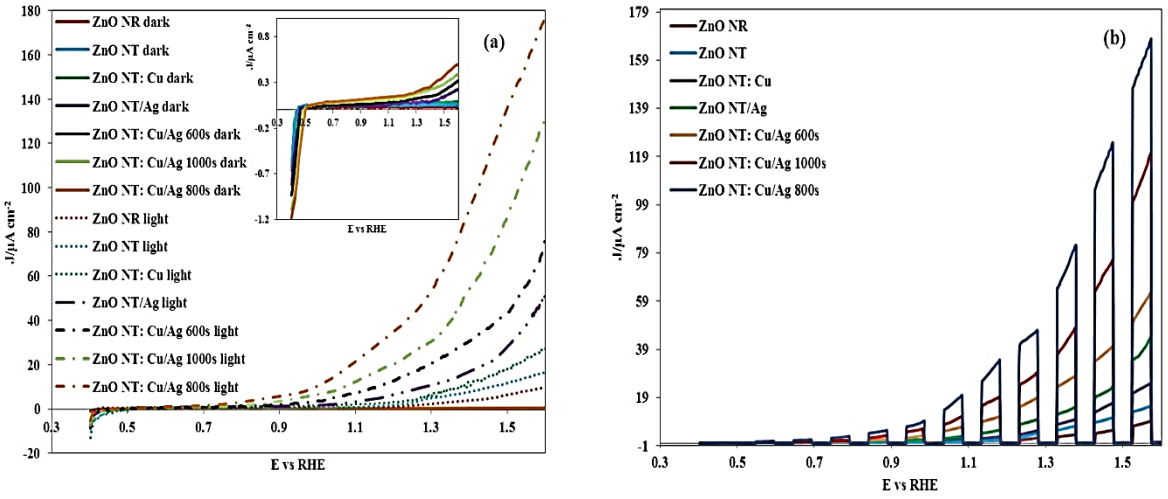

Figure 5. LSV voltammograms (a) dark and visible light conditions of ZnO NRs, ZnO NTs, ZnO NTs: Cu and ZnO NTs: Cu/Ag in 0.5 M Na_2SO_4 solution with scan rate 10 mV/s in the potential window from 0.4 to 1.6 V vs RHE (inset during dark conditions), (b) Under chopped illumination of ZnO NRs, ZnO NTs, ZnO NTs: Cu and ZnO NTs: Cu/Ag in 0.4 to 1.6 V vs RHE

Table 2. Comparison of the present research study with published reports including graphene oxide and zinc oxide

Ref.	Method	Electrolyte	System Of Anodic	Current Density ($mA\ cm^{-2}$)	Light Source
[64]	sol-gel, thermal evaporator and annealing at a high temperature	0.5 M Na_2SO_4	Cu-doped ZnO NRs decorated with Au NPs	0.01 (at 1.2 V vs RHE)	150 W Xenon lamp
[65]	Electrochemical deposition and Hydrothermal	0.5 M Na_2SO_3	Au nanoparticles and Cu_2O nanocrystals decorated on ZnO NTs	0.14 (at 1.1 V vs RHE)	100 mW/cm^2 Xenon lamp
This work	Electrodeposition	0.5 M Na_2SO_4	Cu doping and Ag decoration on the ZnO NTs	0.18 (at 1.6 V vs RHE)	5 mW/cm^2 LED

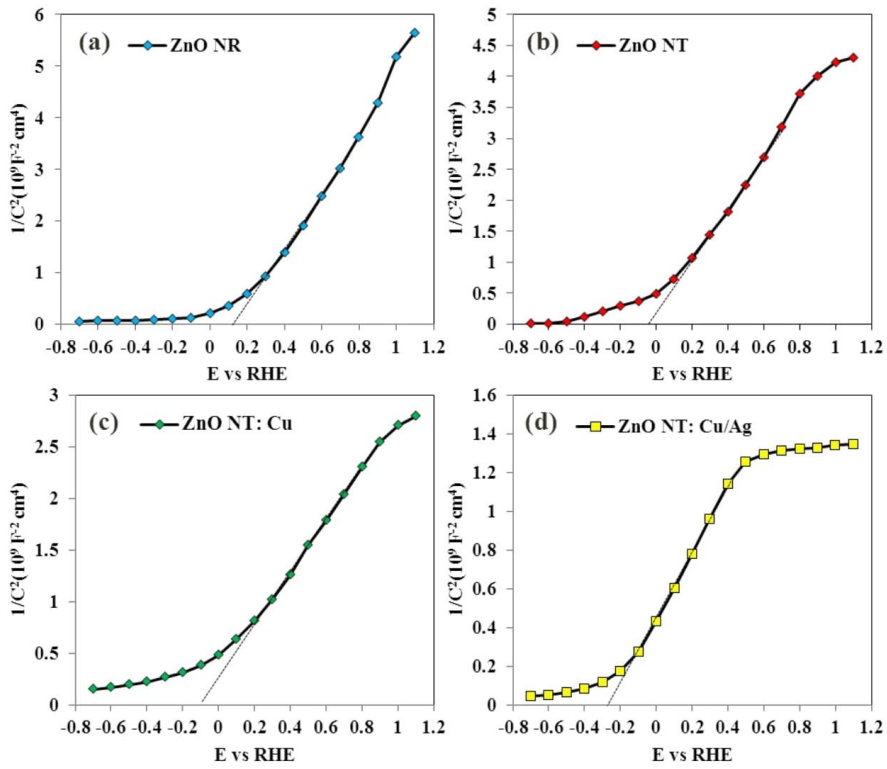

Figure 6. Mott–Schottky plots of (a) pure ZnO NRs, (b) ZnO NTs, (c) ZnO NTs: Cu NTs and (d) ZnO NTs: Cu/Ag in 0.5 M Na_2SO_4 solution during dark conditions

Mott-Schottky analysis was performed to determine the key performance parameters of semiconductors, including flat band potential (V_{fb}), charge carrier density and nature of the conductivity. As can be seen in Figure 6, the slope of the Mott-Schottky plots is positive and

confirms the n-type nature of the films. The carrier densities and V_{fb} of photoanodes are obtained from the slopes and intercept on the voltage axis, respectively. The results are calculated and summarized in Table 3. In the case of ZnO NTs: Cu/Ag photoanode, an increased electron density was observed compared to other cases, leading to improved PEC efficiency [55-57]. The V_{fb} of ZnO NR, ZnO NT, ZnO NT: Cu and ZnO NT: Cu/Ag photoanodes are 0.16, -0.03, -0.11 and -0.28 V respectively. As observed, the V_{fb} of the ZnO NTs: Cu/Ag photoanode changes to the negative values compared with other prepared films, which demonstrates the better ability of photoanode to efficiently separation charge carriers [58,59].

Table 3. Charge carrier density and flat band potential of samples obtained from Mott-Schottky plots

Sample	**N_d (cm^{-3})**	**V_{fb} (V)**
ZnO NRs	3.04×10^{21}	0.16
ZnO NTs	3.91×10^{21}	-0.03
ZnO NTs: Cu	6.74×10^{21}	-0.11
ZnO NTs: Cu/Ag	1.03×10^{22}	-0.28

EIS analyse was done to obtain beneficial information on the electron transfer kinetic and recombination of the synthesized photoanodes. Figure 7 represents the Nyquist plots of photoanodes under dark and visible light irradiation. Also, Figure 7e shows the equivalent circuit of the samples. This circuit includes an ohmic resistance of electrolyte solution (R_s in series with R_{ct} and CPE), the resistance of interfacial charge transfer across the electrode/electrolyte (R_{ct}), and a capacitance for the double–layer and the constant phase element for the electrode/electrolyte interface (CPE).

Table 4. Charge transfer resistance of samples in dark and light conditions

Sample	**R_{ct}/Ω dark**	**R_{ct}/Ω light**
ZnO NRs	223.4	87.2
ZnO NTs	196.4	66.4
ZnO NTs: Cu	134.3	41.1
ZnO NTs: Cu/Ag	100.3	17.6

The Nyquist plot of all photoelectrodes reveals a semicircle, which is related to the charge transfer process at the photoanode/electrolyte interface, and its diameter is equal to the R_{ct}. The R_{ct} values for all the prepared samples under dark and illumination are listed in Table 4. It can be inferred from the Nyquist plots that a lower value of R_{ct} displays a more efficient charge transfer across the electrode/electrolyte interface under illumination and reduces the possibility of charge recombination [60]. Among all the photoanodes, ZnO NTs: Cu/Ag reveals the lowest R_{ct} value (17.6 Ω), which is responsible for the best PEC performance. Therefore, Cu doping and Ag decoration on the ZnO NTs structure effectively improved the charge transfer.

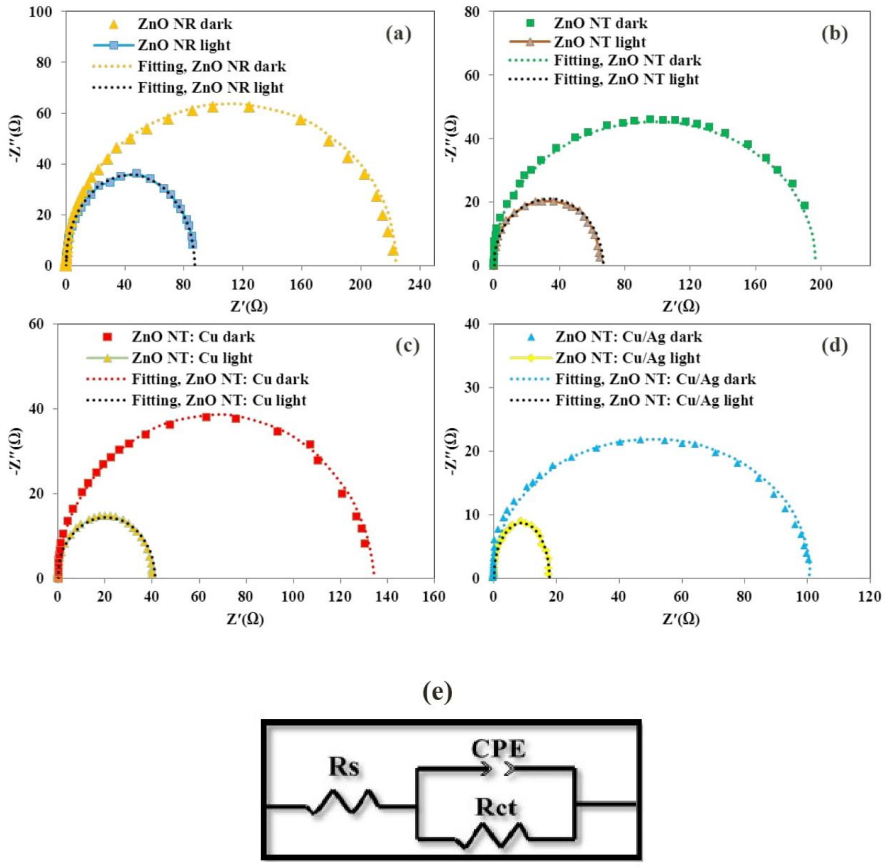

Figure 7. Nyquist plots of electrochemical impedance spectra a) pure ZnO NRs, b) ZnO NTs, c) ZnO NTs: Cu and (d) ZnO NTs: Cu/Ag in the dark and light conditions, respectively, e) Equivalent circuits of photoanodes

3.4. Mechanism of PEC water oxidation

In order to investigate the separation and charge transfer mechanism in ZnO NT: Cu/Ag photoanode, a possible schematic diagram is shown in Figure 8. Under visible light irradiation with higher energy than the ZnO NTs: Cu/Ag band gap, electrons are excited and transferred from the valence band to the conduction band of ZnO, leaving positively charged holes in the valence band. Since the Fermi level of Ag is lower than that of ZnO, in ZnO NT: Cu/Ag

photoanode, the Fermi levels are realigned between the Ag NPs/ZnO interface (the Fermi level of Ag has an up shift, while ZnO has a down shift) [61]. As a result, a space charge region is formed between the interface of ZnO and Ag, and an internal electric field is generated at the interface of ZnO and Ag. On the other hand, Ag NPs increase the electron concentration in the conduction band of ZnO based on the LSPR effect. Under visible light, Ag NPs interact with the incident light and lead to collective oscillation of resonant excited electrons, which enhances visible absorption [30,62]. Therefore, the light absorption spectra are enlarged and the plasmon-induced hot electrons with energy higher than Schottky barrier height between ZnO and Ag can transfer to the conduction band of ZnO and increase the carrier density. Then, the electrons excited to the conduction band of ZnO reach the Pt electrode through an external circuit and participate in the reduction of water to form H_2. Besides, the valence band holes of ZnO are depleted by water oxidation to produce O_2 under an applied potential [4,63]. Therefore, the synergistic LSPR performance of Ag NPs and the ability to absorb light as well as the efficient separation and transfer of charge carriers due to the well-band matching between ZnO, Cu and Ag increase the PEC efficiency of ZnO NTs: Cu/Ag compared to other photoanodes.

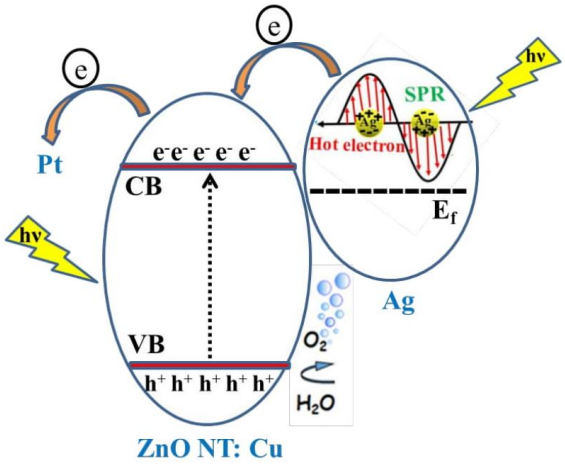

Figure 8. Electron transfer mechanism in ZnO NTs: Cu/Ag photoanode

4. CONCLUSION

In summary, in this work, Cu-doped ZnO NTs decorated with Ag NPs were successfully fabricated through a facile and cost-effective electrodeposition technique for PEC water splitting under visible light illumination. The properties of prepared samples were characterized by different analytical techniques such as FESEM, EDX, XRD, EIS and UV–visible absorption spectroscopy. The results of these findings are in good agreement with each other. The obtained results demonstrate the improvement of PEC performance of ZnO NT: Cu/Ag photoanode in visible light compared to other photoelectrodes. Ag NPs decorated ZnO NTs: Cu display a significant photocurrent density of about180 µA/cm2 at 1.6 V vs. RHE. The

enhancement is mainly attributed to the LSPR effect of Ag NPs and the inherent visible light harvesting property of Cu. Cu doping and Ag decoration on the ZnO NTs greatly increase the light absorption in visible light region, and also facilitate charge transfer and separation and reduce charge recombination rate. Also, EIS measurements illustrate a remarkable reduction in charge transfer resistance down to 17.6 Ω.

Acknowledgments

State The authors gratefully acknowledged the financial support from K.N. Toosi University of Technology (KNTU) in Iran.

Declarations of interest

The authors declare no conflict of interest in this reported work.

REFERENCES

[1] C. Chen, W. Ma, and J. Zhao, Chem. Soc. Rev. 39 (2010) 4206.
[2] Z. Zhang, L. Zhang, M.N. Hedhili, H. Zhang, and P. Wang, Nano Lett. 13 (2013) 14.
[3] S.S. Kalanur, I.H. Yoo, and H. Seo, Electrochim. Acta 254 (2017) 348.
[4] C. Zhang, M. Shao, F. Ning, S. Xu, Z. Li, M. Wei, D.G. Evans, and X. Duan, Nano Energy 12 (2015) 231.
[5] Y. Lu, J. Zhang, L. Ge, C. Han, P. Qiu, and S. Fang, J. Colloid Interface Sci. 483 (2016) 146.
[6] C.M. Fung, J.S. Lloyd, S. Samavat, D. Deganello, and K.S. Teng, Sens. Actuators B Chem. 247 (2017) 807.
[7] A. Kargar, K. Sun, Y.Jing, C. Choi, H. Jeong, G. Y.Jung, S. Jin, and D. Wang, ACS Nano 7 (2013) 9407.
[8] F. Rasouli, A. Rouhollahi, and F. Ghahramanifard, Superlattices Microstruct. 125 (2019) 177.
[9] Z. Li, S. Feng, S. Liu, X. Li, L. Wang, and W. Lu, Nanoscale 7 (2015) 19178.
[10] X. Ren, A. Sangle, S. Zhang, S. Yuan, Y. Zhao, L. Shi, R.L.Z. Hoye, S. Cho, D. Li, and J.L.M. Driscoll, J. Mater. Chem. A 4 (2016) 10203.
[11] A.R. Marlinda, N. Yusoff, A. Pandikumar, N.M. Huang, O. Akbarzadeh, S. Sagadevan, Y.A. Wahab, and M.R. Johan, Int. J. Hydrogen Energy 44 (2019) 17535.
[12] S. Khanchandani, S. Kundu, A. Patra, and A.K. Ganguli, J. Phys. Chem. C 116 (2012) 23653.
[13] M. Ahmad, and J. Zhu, J. Mater. Chem. 21 (2011) 599.
[14] Y. Qiu, K. Yan, H. Deng, and S. Yang, Nano Lett. 12 (2012) 407.

[15] F. Achouri, S. Corbel, L. Balan, K. Mozet, E. Girot, G. Medjahdi, M.B. Said, A. Ghrabi, and R. Schneider, Mater. Des. 101 (2016) 309.
[16] X. Zhang, Y. Liu, and Z. Kang, ACS Appl. Mater. Interfaces 6 (2014) 4480.
[17] Z. Bai, X. Yan, Y. Li, Z. Kang, S. Cao, and Y. Zhang, Adv. Energy Mater. 6 (2016) 1501459.
[18] Y. Mao, H. Yang, J. Chen, J. Chen, Y. Tong, and X. Wang, Nano Energy 6 (2014) 10.
[19] W. Liu, Y.Y. Liu, J.S. Do, and J. Li, Appl. Surf. Sci. 390 (2016) 929.
[20] A. Cai, X. Wang, Y. Qi, and Z. Ma, Appl. Surf. Sci. 391 (2017) 484.
[21] R. Saleh, and N.F. Djaja, Spectrochim. Acta Part A 130 (2014) 581.
[22] M. Pashchanka, R. Hoffmann, A. Gurlo, J. Swarbrick, J. Khanderi, J. Engstler, A. Issanin, and J.J. Schneider, Dalton Trans. 40 (2011) 4307.
[23] M. Eron, and A. Rothwarf, J. Appl. Phys. 57 (1985) 2275.
[24] X. Zhou, Z.T. Gossage, B.H. Simpson, J. Hui, Z.J. Barton, and J. Rodriguez-Lopez, ACS Nano 10 (2016) 9346.
[25] W. Hou, and S.B. Cronin, Adv. Funct. Mater. 23 (2013) 1612.
[26] H. Dotan, O. Kfir, E. Sharlin, O. Blank, M. Gross, I. Dumchin, G. Ankonina, and A. Rothschild, Nat. Mater. 12 (2013) 158.
[27] Q.Q. Chang, Y.W. Cui, H.H. Zhang, F. Chang, B.H. Zhu, and S.Y. Yu, RSC Adv. 9 (2019) 12689.
[28] C. Peng, W. Wang, W. Zhang, Y. Liang, and L. Zhuo, Appl. Surf. Sci. 420 (2017) 286.
[29] F. Rasouli, A. Rouhollahi, and F. Ghahramanifard, Mater. Sci. Semicond. Process. 93 (2019) 371.
[30] S. Linic, P. Christopher, and D.B. Ingram, Nat. Mater. 10 (2011) 911.
[31] S.C. Warren, and E. Thimsen, Energy Environ. Sci. 5 (2012) 5133.
[32] N.J. Halas, S. Lal, W.S. Chang, S. Link, and P. Nordlander, Chem. Rev. 111 (2011) 3913.
[33] Y. Tian, and T. Tatsuma, J. Am. Chem. Soc. 127 (2005) 7632.
[34] S. Mubeen, G. Hernandez-Sosa, D. Moses, J. Lee, and M. Moskovits, Nano Lett. 11 (2011) 5548.
[35] M. Prasad, V. Sharma, R. Aher, A. Rokade, P. Ilaiyaraja, C. Sudakar, and S. Jadkar, J. Mater. Sci. 52 (2017) 13572.
[36] D. Zhang, Y. Tang, F. Jiang, and Z. Han, J. Chen, Appl. Surf. Sci. 369 (2016) 178.
[37] C.J. Jia, L.D. Sun, Z.G. Yan, L.P. You, F. Luo, X.D. Han, Y.C. Pang, Z. Zhang, and C.H. Yan, Angew. Chem. Int. Ed. 117 (2005) 4402.
[38] F. Li, Y. Ding, P.X. Gao, X.Q. Xin, and Z.L. Wang, Angew. Chem. Int. Ed. 43 (2004) 5238.
[39] L. Vayssieres, K. Keis, A. Hagfeldt, and S.E. Lindquist, Chem. Mater. 13 (2001) 4395.

[40] G.W. She, X.H. Zhang, W.S. Shi, J.C. Chang, C.S. Lee, S.T. Lee, and C.H. Liu, Appl. Phys. Lett. 92 (2008) 053111.
[41] C. Das, P. Roy, M. Yang, H. Jha, and P. Schmuki, Nanoscale 3 (2011) 3094.
[42] T. Pauporté, and D. Lincot, J. Electroanal. Chem. 517 (2001) 54.
[43] A.K. Singh, G.S. Thool, R.S. Singh, and S.P. Singh, J. Alloys Compd. 618 (2015) 421.
[44] M. Ashokkumar, and S. Muthukumaran, Opt. Mater. 37 (2014) 671.
[45] A. Rokade, S. Rondiyal, V. Sharma, M. Prasad, H. Pathan, and S. Jadkar, J. Solid State Electrochem. 21 (2016) 2639.
[46] M. Wang, F. Ren, J. Zhou, G. Cai, L. Cai, Y. Hu, D. Wang, Y. Liu, L. Guo, and S. Shen, Sci. Rep. 5 (2015) 12925.
[47] Y. K. Hsu, and C.M. Lin, Electrochim. Acta 74 (2012) 73.
[48] P. Jongnavakit, P. Amornpitoksuk, S. Suwanboon, and N. Ndiege, Appl. Surf. Sci. 258 (2012) 8192.
[49] Y. Wei, J. Kong, L. Yang, L. Ke, H.R. Tan, H. Liu, Y. Huang, X.W. Sun, X. Lu, and H. Du, J. Mater. Chem. A 1 (2013) 5045.
[50] M. Mittal, M. Sharma, and O.P. Pandey, Sol. Energy 110 (2014) 386.
[51] S.S. Xu, H.L. Lu, Y. Zhang, T. Wang, Y. Geng, W. Huang, S.J. Ding, and D.W. Zhang, J. Alloys Compd. 638 (2015) 133.
[52] K.S. Ahn, T. Deutsch, Y. Yan, C.S. Jiang, C.L. Perkins, J. Turner, and M. Al-Jassim, J. Appl. Phys. 102 (2007) 023517.
[53] X. Luan, and Y. Wang, J. Mater. Sci. Technol. 30 (2014) 1.
[54] M.Z. Ge, C.Y. Cao, S.H. Li, Y.X. Tang, L.N. Wang, N. Qi, J.Y. Huang, K.Q. Zhang, S.S. Al-Deyabe, and Y.K. Lai, Nanoscale 8 (2016) 5226
[55] J.G. Yu, Q.J. Xiang, M.H. Zhou, Appl. Catal. B Environ. 90 (2009) 595.
[56] B. Liu, H.M. Chen, C. Liu, S.C. Andrews, C. Hahn, P.D. Yang, Large-scale synthesis of transition-metal-doped TiO_2 nanowires with controllable overpotential, J. Am. Chem. Soc. 135 (2013) 9995.
[57] X.F. Cheng, W.H. Leng, D.P. Liu, Y.M. Xu, J.Q. Zhang, and C.N. Cao, J. Phys. Chem. C 112 (2008) 8725.
[58] J. Zhang, J.H. Bang, C. Tang, and P.V. Kamat, ACS Nano 4 (2009) 387.
[59] J. Zhua, W. Lia, J. Lia, Y. Lia, H. Hua, and Y. Yang, Electrochim. Acta 112 (2013) 191.
[60] C.Y. Lin, Y.H. Lai, D. Mersch, E. Reisner, Chem. Sci. 3 (2012) 3482.
[61] H.M. Chen, C.K. Chen, C.J. Chen, L.C. Cheng, P.C. Wu, B.H. Cheng, Y.Z. Ho, M.L. Tseng, Y.Y. Hsu, T.S. Chan, J.F. Lee, R.S. Liu, and D.P. Tsai, ACS Nano 6 (2012) 7362.
[62] C. Clavero, Photonics 8 (2014) 95.
[63] Z. Bai, X. Yan, Z. Kang, Y. Hu, X. Zhang, and Y. Zhang, Nano Energy 14 (2015) 392.

[64] H.Q. Huynh, K.N. Pham, B.T. Phan, C.K. Tran, H. Lee, and V.Q. Dang, J. Photochem. Photobiol. A. 399 (2020) 112639.

[65] S. Fu, J. Chen, H. Han, W. Wang, H. Shi, J. Fu, and Y. Jia, J. Alloys Compd.799 (2019) 183.